The Symmetry of Ordered Cubic γ-Fe_2O_3 Investigated by TEM

Klemens Kelm and Werner Mader

Institut für Anorganische Chemie der Rheinischen Friedrich-Wilhelms-Universität Bonn, Römerstraße 164, D-53117 Bonn, Germany

Reprint requests to Prof. Dr. W. Mader. Fax +49 (0)228 / 734205. E-mail: mader@uni-bonn.de

Z. Naturforsch. **61b,** 665 – 671 (2006); received November 14, 2005

Dedicated to Professor Wolfgang Jeitschko on the occasion of his 70th birthday

Well-crystallized particles of cubic and tetragonal γ-Fe_2O_3 embedded in a Pd matrix were produced besides other oxides by internal oxidation of a Pd-Fe alloy in air. Particles of tetragonal γ-Fe_2O_3 consist of orientation domains with the *c* axes normal to each other. Particles of the ordered cubic γ-Fe_2O_3 appear single crystalline in bright field and in dark field images with reflections of the basic spinel structure. In dark field images enantiomorphous domains were observed using reflections of the ordered phase. From the analysis of electron diffraction patterns in the principal zone axes the description of ordered cubic γ-Fe_2O_3 in the enantiomorphous space groups $P4_132/P4_332$ follows without further presumptions. In the sequence from space group $Fd\bar{3}m$ of disordered cubic γ-Fe_2O_3 *via* $P4_132/P4_332$ of the ordered cubic phase to the pair $P4_12_12/P4_32_12$ of tetragonal γ-Fe_2O_3 a continuous group-subgroup relation can be derived. This relation shows that ordered cubic γ-Fe_2O_3 is an intermediate phase upon ordering of vacant octahedral sites towards tetragonal γ-Fe_2O_3.

Key words: γ-Fe_2O_3, Symmetry, Electron Diffraction, Enantiomorphism, Internal Oxidation, Domain Contrast

Introduction

Among the various iron oxides, γ-Fe_2O_3 has attracted much attention because of its useful and technologically important properties [1]. γ-Fe_2O_3 is metastable with respect to α-Fe_2O_3. In pure powders the γ-$Fe_2O_3 \rightarrow \alpha$-$Fe_2O_3$ transformation temperature is approximately 400 °C [1] while particles embedded in a SiO_2 matrix have been observed to exist up to 1400 °C [2]. γ-Fe_2O_3 has a defect spinel structure that can be derived from magnetite (Fe_3O_4, space group $Fd\bar{3}m$) by removing up to $1/9$ of the iron atoms [3].

As early as 1939, superstructure reflections forbidden in space group $Fd\bar{3}m$ were observed in some γ-Fe_2O_3 samples [4]. Later, a structure similar to $LiFe_5O_8$ was proposed for γ-Fe_2O_3 where the vacancies in the iron oxide are located at the positions occupied by lithium in the ferrate. Thus, the space group was assumed to be either $P4_132$ or the enantiomorphous one, $P4_332$ [5]. Some years later, a splitting of the superstructure reflections was observed resulting in a tripled tetragonal cell. Based on X-ray data, symmetry of either $P4_1$ or $P4_3$ was proposed [6].

The origin of the superstructures has been identified as an ordering of iron vacancies at octahedral sites of the spinel structure [7 – 9]. The appearance of the ordering depends on the degree of the iron deficit [10, 11] as well as on the particle size of the material [8, 12]. Structural refinements on tetragonal γ-Fe_2O_3 confirm the enantiomorphous pair $P4_12_12/P4_32_12$ as space groups; while atomic coordinates for cubic [12, 14] or tetragonal subcells [13] are given as intermediate results of the refinement procedure. Symmetry investigations by convergent beam electron diffraction suggested a point group $m\bar{3}m$ and a cubic cell with a tripled lattice parameter [15], possibly representing a further ordering.

On the basis of lattice parameter measurements, a continuous solid solution series from Fe_3O_4 *via* ordered cubic γ-Fe_2O_3 towards tetragonal γ-Fe_2O_3 has been reported [11, 32].

Unfortunately, there is some ambiguity about the symmetry of the ordered cubic variant of γ-Fe_2O_3. Several space groups based on powder diffraction data have been published over the years: $P2_13$ [16], $P\bar{4}3m$ [17] and $P4_132$ [18]. It has been shown that studies based on powder samples are always hampered by the presence of additional phases [20]. Sometimes, the problems arise from the measurement itself: For one particular sample, it has been reported that the

tetragonal splitting was clearly observed in electron diffraction, whereas this splitting was not revealed in synchrotron measurements without using anomalous dispersion [12]. The simultaneous presence of enantiomorphous domains in a natural specimen was detected by means of contrast experiments in the transmission electron microscope. While the domain structure observed for γ-Fe_2O_3 was identical to the domain structure observed for $LiFe_5O_8$ with space groups $P4_132/P4_332$ applicable simultaneously, it was concluded that both compounds are of the same symmetry [19]. The procedure preformed did not account for the formerly proposed space group $P2_13$ [16] which was left out of consideration. Hence, uncertainties concerning the space group of ordered cubic γ-Fe_2O_3 still existed.

In the present study internal oxidation [26] of a Pd-Fe alloy was used for synthesis of the Fe-O phases. This unusual method yielded isolated iron oxide crystals embedded in the palladium matrix. Their size frequently exceeded 1 μm. The crystals were ideal for imaging and diffraction analysis in the transmission electron microscope. This material allowed us to determine the symmetry as well as the domain structure of γ-Fe_2O_3, thus avoiding the problems associated with space group determination by powder methods. The results are discussed with respect to previous findings in the literature.

Material Synthesis and Experimental Techniques

A number of different approaches have been published for the synthesis of γ-Fe_2O_3. The dehydration of γ-FeOOH as well as the oxidation of magnetite are the most commonly used routes [21]. Other successful methods are *e. g.* the decomposition of organic iron salts [22], spray pyrolysis [23], oxidation of iron in an electric discharge [4, 24], and decomposition of Si/Fe/O containing gels [25].

Internal oxidation is applicable if the diffusion coefficient of oxygen in the base metal is higher than the diffusion coefficient of the solute in the base metal, as in the case of the Pd-Fe-O system [27]. Oxide precipitates form inside the metallic matrix under the condition that the partial pressure of oxygen is adequate to oxidize the solute metal without oxidising the solvent metal. These conditions are fulfilled in the system Pd-Fe-O at temperatures exceeding 800 °C.

The alloy ($Pd_{96}Fe_4$) was cold-rolled to sheets of a final thickness of 100 μm. The subsequent homogenisation and recrystallization was carried out in sealed silica tubes under vacuum.

For oxidation, the alloy sheets were placed in corundum boats in a way such that the contact area of metal and boat was minimized to ensure homogeneous access of oxygen to the sheet's surface. These boats were placed in a hot tube furnace in air for internal oxidation. The reaction time was 24 h at temperatures between 900 °C and 1200 °C. The samples were removed from the hot furnace and immediately quenched in liquid nitrogen.

For the investigation by transmission electron microscopy (TEM), punched discs of the material were thinned mechanically to a final thickness of 30 – 40 μm. Final thinning was achieved by Ar^+ ion beam etching at 4 – 6 keV and 7.5° angle of incidence.

Two different microscopes were used for the investigations: A Philips EM400T operated at an accelerating voltage of 120 keV which gave access to large tilt angles and a Philips CM30ST operated at an accelerating voltage of 300 keV. The CM30ST microscope is equipped with a Noran HPGe energy dispersive X-ray detector which allows quantitative analysis of elements with $Z = 11$ with a detection limit of approx. 0.5 at.-%.

Results

The iron oxides precipitated as facetted crystals within the palladium matrix (Fig. 1). The different iron oxide modifications (Table 1) were identified by selected area electron diffraction (SAED). Impurities in the precipitated particles were below the detection limit of the energy dispersive X-ray analysis system. The on-axis SAED-patterns of the individual particles

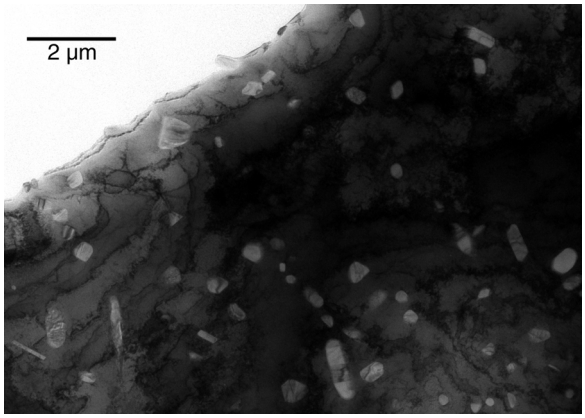

Fig. 1. TEM image of iron oxide particles obtained by internal oxidation of a $Pd_{96}Fe_4$ alloy.

Table 1. Iron oxides observed at different preparation temperatures.

Oxidation temperature (°C)	Observed phases
900	Fe_3O_4, α-, β-, γ-, ε-Fe_2O_3
1000	α-, β-, γ-, ε-Fe_2O_3
1100	Fe_3O_4, α-, β-, γ-, ε-Fe_2O_3
1200	γ-, ε-Fe_2O_3

were indexed on the basis of published powder X-ray data and of lattice parameters for α-Fe_2O_3, β-Fe_2O_3, cubic γ-Fe_2O_3, tetragonal γ-Fe_2O_3 and Fe_3O_4 [28]. Lattice parameters for ε-Fe_2O_3 were taken from reference [33]. Lattice parameters for all oxides investigated agreed with the literature data within the accuracy of SAED. While the identification of the modifications α-, β- and ε-Fe_2O_3 was straight forward, more care had to be taken in the case of the spinel-related oxides Fe_3O_4 and γ-Fe_2O_3. Magnetite was identified by the reversible Verwey transition at 119 K [29], which was observed *in situ* in the transmission electron microscope using a liquid nitrogen cooled specimen holder. All investigated crystals giving diffraction patterns compatible with the basic spinel structure showed the Verwey transition. Thus, we conclude that no face centred cubic γ-Fe_2O_3 was present. Primitive cubic γ-Fe_2O_3 was distinguished from tetragonal γ-Fe_2O_3 by tilting in a $\langle uv0 \rangle$ orientation, which allowed the observation of the $\{00l\}$ superstructure reflections or by analysis of the diameter of higher order Laue zones (HOLZ). Most particles appeared to be single-crystalline by morphology (Fig. 1). Twinning was present in a few Fe_3O_4 and cubic γ-Fe_2O_3 crystals (spinel law) as well as occasionally in ε-Fe_2O_3. All tetragonal γ-Fe_2O_3 particles were found to exist as domains with different *c*-axis orientations. Most of the cubic oxides showed a cube-on-cube orientation relationship with respect to the palladium matrix.

Because of inconsistencies in the published data, the space group symmetry of cubic γ-$Fe_2O_3$was investigated in detail. Electron diffraction patterns in [100], [110] and [111] orientation were recorded from selected crystals (Fig. 2a – c). Patterns were recorded with reduced beam intensity since degradation of the superstructure reflections was observed at high electron doses. The presence of reflections (*hkl*) with $h+k=2n+1$, $h+l=2n+1$ and $k+l=2n+1$ is not compatible with face centred cubic symmetry of the basic spinel type while the observation of reflections $h+k+l=2n+1$ exclude a body centred lattice. Since reflections with $k+l=2n+1$ were observed in [100] orientation, the presence of *n* or *d* glide planes perpendicular to the *a* axis can be ruled out. Furthermore, the

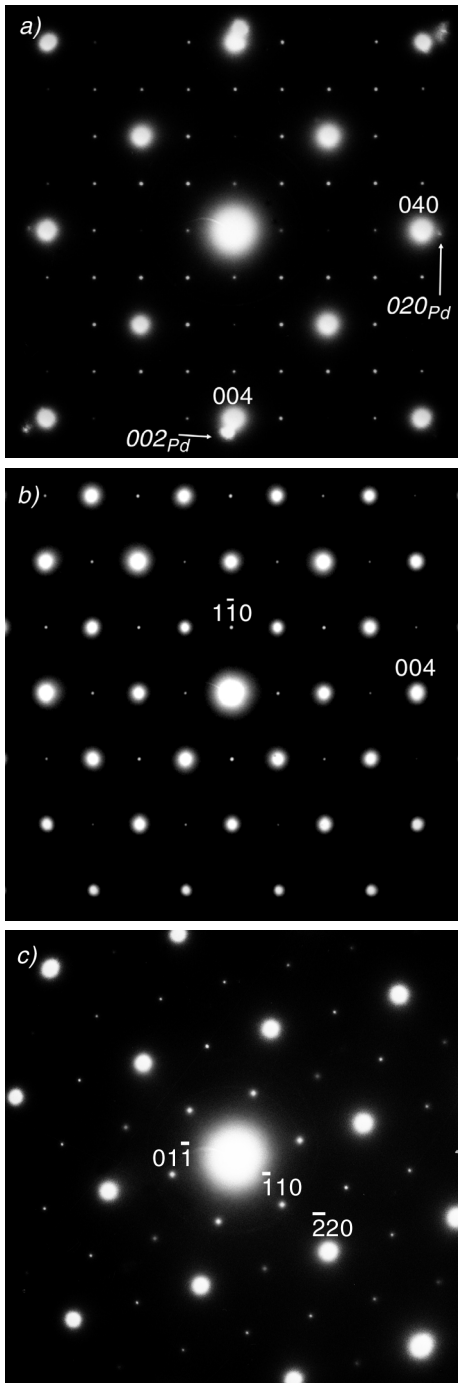

Fig. 2. Electron diffraction patterns of cubic γ-Fe_2O_3 in principal zone axes: [100] (a), [110] (b), [111] (c). Forbidden reflections of type 00*l* are caused by Umweganregung.

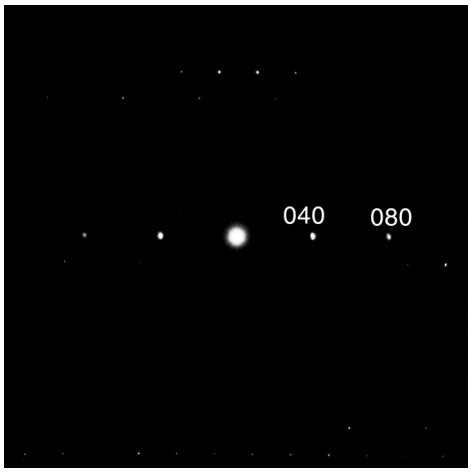

Fig. 3. Electron diffraction pattern of cubic γ-Fe_2O_3 tilted about [010] to prevent Umweganregung.

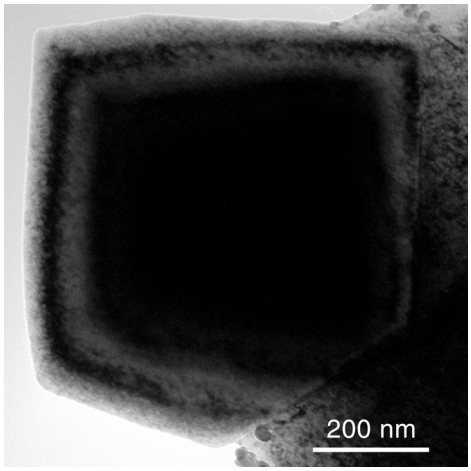

Fig. 4. Bright field micrograph of a cubic γ-Fe_2O_3 particle, beam direction is [111].

presence of *a* glide planes normal to $\langle 100 \rangle$ is ruled out by the presence of reflections $(0kl)$, $k = 2n+1$. The existence of glide planes perpendicular to $\langle 110 \rangle$ is excluded by the presence of reflections (hhl), $l = 2n+1$ in the [110] zone axis. Thus, the extinction symbol is P---, $P2_1$--, $P4_2$-- or $P4_1$--. The absence of glide planes is proven by the lack of periodicity differences between the zero order Laue zones (ZOLZ) and first order Laue zones (FOLZ) in [100] and [110] direction, while the observed shift of the reflections between ZOLZ and FOLZ in these orientations is expected for a primitive lattice without glide planes [30], again yielding P---, $P2_1$--, $P4_2$-- or $P4_1$-- as possible extinction symbols. This leaves $P23$, $Pm\bar{3}$, $P432$, $P\bar{4}3m$ and

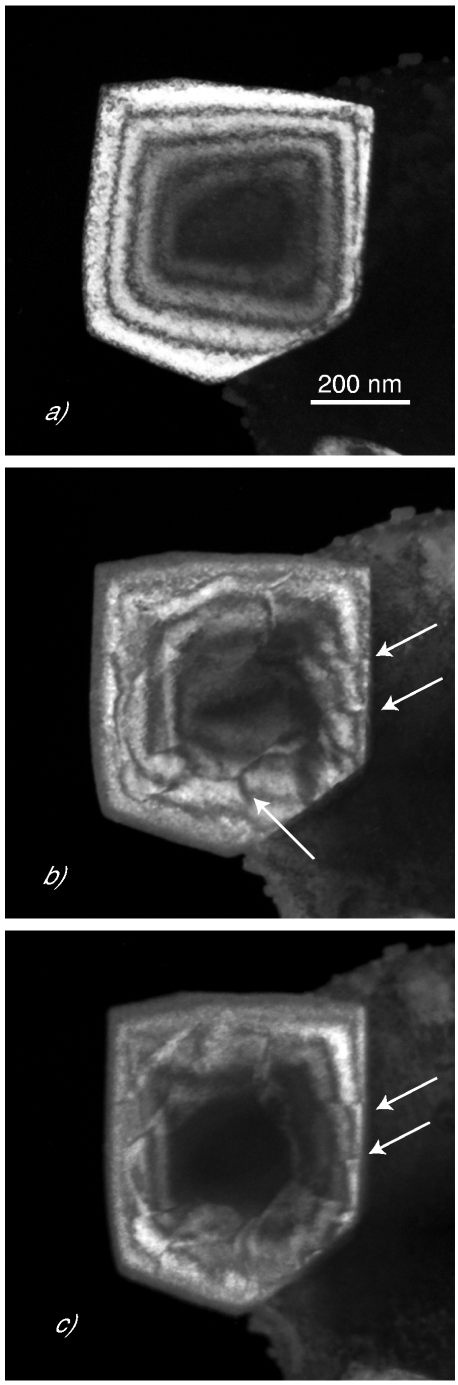

Fig. 5. Dark field micrographs of a cubic γ-Fe_2O_3 particle. Operating reflections are $(\bar{2}20)$ (a), (110) (b) and $(0\bar{1}1)$ (c). Inversion domain boundaries are indicated by arrows.

$Pm\bar{3}m$ as well as $P2_13$, $P4_232$ and the enantiomorphous pair $P4_132/P4_332$ as possible space groups. The

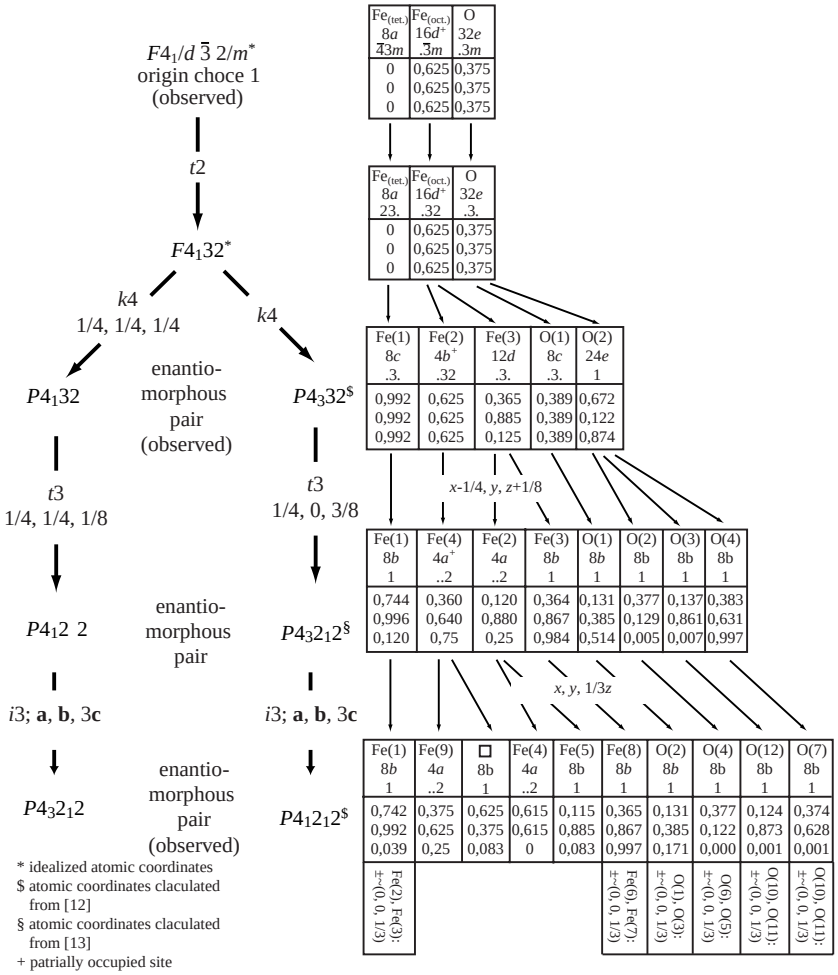

$Fe_{(tet.)}$ 8*a* $\bar{4}3m$	$Fe_{(oct.)}$ 16d^+ .3*m*	O 32*e* .3*m*
0	0,625	0,375
0	0,625	0,375
0	0,625	0,375

$Fe_{(tet.)}$ 8*a* 23.	$Fe_{(oct.)}$ 16d^+ .32	O 32*e* .3.
0	0,625	0,375
0	0,625	0,375
0	0,625	0,375

Fe(1) 8*c* .3.	Fe(2) 4b^+ .32	Fe(3) 12*d* .3.	O(1) 8*c* .3.	O(2) 24*e* 1
0,992	0,625	0,365	0,389	0,672
0,992	0,625	0,885	0,389	0,122
0,992	0,625	0,125	0,389	0,874

Fe(1) 8*b* 1	Fe(4) 4a^+ ..2	Fe(2) 4*a* ..2	Fe(3) 8*b* 1	O(1) 8*b* 1	O(2) 8b 1	O(3) 8b 1	O(4) 8b 1
0,744	0,360	0,120	0,364	0,131	0,377	0,137	0,383
0,996	0,640	0,880	0,867	0,385	0,129	0,861	0,631
0,120	0,75	0,25	0,984	0,514	0,005	0,007	0,997

Fe(1) 8*b* 1	Fe(9) 4*a* ..2	□ 8b 1	Fe(4) 4*a* ..2	Fe(5) 8b 1	Fe(8) 8*b* 1	O(2) 8*b* 1	O(4) 8b 1	O(12) 8b 1	O(7) 8b 1
0,742	0,375	0,625	0,615	0,115	0,365	0,131	0,377	0,124	0,374
0,992	0,625	0,375	0,615	0,885	0,867	0,385	0,122	0,873	0,628
0,039	0,25	0,083	0	0,083	0,997	0,171	0,000	0,001	0,001
Fe(2), Fe(3): ±~(0, 0, 1/3)					Fe(6), Fe(7): ±~(0, 0, 1/3)	O(1), O(3): ±~(0, 0, 1/3)	O(6), O(5): ±~(0, 0, 1/3)	O(10), O(11): ±~(0, 0, 1/3)	O(10), O(11): ±~(0, 0, 1/3)

Fig. 6. Group-subgroup relationships between space groups known for the different forms of γ-Fe_2O_3. The boxes on the right hand side contain the element, Wyckoff position, site symmetry and atomic coordinates *x*, *y*, *z*.

first five of these can be distinguished from the latter four ones by the extinction of reflections due to the presence of screw axes.

Since iron oxide is a strong scatterer for electrons, the dynamic diffraction effects present (Fig. 2a) have to be considered. For this reason, the extinction of reflections $\{0k0\}$, $k = 2n+1$ or $k = 4n+1$ was examined by tilting a crystal out off the [100] orientation about the [010] axis so that Umweganregung of kinematically forbidden reflections of type $(0k0)$ is prevented. The exclusive presence of spots with $k = 4n$ in this row of reflections (Fig. 3) proves the existence of either a 4_1 or 4_3 screw axis, leaving the enantiomorphous pair $P4_132/P4_332$ as the only space groups possible for ordered cubic γ-Fe_2O_3.

The question arising from this result was whether the particles consist of single domains or may be composed of different domains with both space groups simultaneously present. Attempts failed to solve this question by convergent beam electron diffraction (CBED). Since the superstructure reflections vanished within seconds, we were unable to record a useful convergent diffraction pattern even at the lowest possible electron dose in our transmission electron microscope. Thus, a diffraction contrast experiment in imaging mode was carried out. A contrast difference across a domain boundary separating enantiomorphous domains can be observed in dark field microscopy under multiple beam imaging conditions [31]. Best contrast was achieved by tilting the crystal so that only

one systematic row of reflections was excited. In bright field imaging, the crystal exhibits continuous thickness fringes running along its outline, indicating lines of equal thickness in beam direction (Fig. 4). A dark field image of the same crystal using $(\bar{2}20)$ as operating reflection is shown in Fig. 5a. The reflection $(\bar{2}20)$ is allowed for the basic spinel structure. Again, continuous thickness fringes are obtained as expected from diffraction theory. By using $(\bar{1}10)$ or $(01\bar{1})$ as operating reflection for dark field imaging, discontinuities in thickness contours are observed. These reflections originate due to the ordering of the vacant octahedral atom positions, thus being sensitive to the space groups of the domains. An abrupt change in contrast is visible across the domain boundary separating the domains of the two space groups (Fig. 5b and Fig. 5c). Hence, cubic γ-Fe_2O_3 particles consist of domains having the two enanthiomorphous space groups, $P4_132$ and $P4_332$.

Discussion and Conclusion

Several investigations concerning the crystal symmetry of cubic γ-Fe_2O_3 are reported in the literature, leading to different proposals for its space group [4, 5, 16 – 19]. It was found that the examination of crystal symmetry was inherently difficult using powder diffraction methods due to materials inhomogeneity [20] and the limited suitability of the method applied [12]. To overcome these problems, we used single crystal electron diffraction capable of recording diffraction patterns containing reflections of even very faint intensity from sub micrometer sized particles.

The space groups observed for γ-Fe_2O_3, $P4_132/P4_332$, are subgroups of the space group of magnetite as well as of the disordered γ-Fe_2O_3, *i. e.* $Fd\bar{3}m$. Furthermore, the enantiomorphous space groups observed for tetragonal γ-Fe_2O_3, $P4_12_12/P4_32_12$ are subgroups of the space groups found for ordered cubic γ-Fe_2O_3. It is possible to construct a continuous group-subgroup relation between disordered and tetragonal γ-Fe_2O_3 (Fig. 6). The preliminary atomic coordinates resulting from the refinement of tetragonal γ-Fe_2O_3 in cubic symmetry [12, 14] are assumed to be a good approximation for the atomic coordinates of ordered cubic γ-Fe_2O_3. With these atomic parameters this material fits into this group-subgroup relationship (Fig. 6).

This relationship should be expected for a continuous transition between the various iron oxides, as it was found earlier on the basis of the lattice parameters as a function of composition [11]. One of the space groups published for ordered cubic γ-Fe_2O_3 was $P\bar{4}3m$ [17]. While in principle the construction of a continuous group-subgroup relationship between the space groups $Fd\bar{3}m$ and $P\bar{4}3m$ is possible ($Fd\bar{3}m$—$t2 \rightarrow F\bar{4}3m$—$k4 \rightarrow P\bar{4}3m$), the space group $P\bar{4}3m$ is not a supergroup of the space groups $P4_12_12/P4_32_12$. From the above considerations it would follow that ordered cubic γ-Fe_2O_3 is a separate modification besides tetragonal γ-Fe_2O_3. Furthermore, space group $P2_13$, proposed for γ-Fe_2O_3 [16] also would have established cubic γ-Fe_2O_3 as a separate modification besides the tetragonal γ-Fe_2O_3 since $P2_13$ is a subgroup of $P4_132/P4_332$ ($P4_332$—$t2 \rightarrow P2_13$), but is neither a supergroup nor a subgroup of $P4_12_12/P4_32_12$.

Our observations confirm that ordered cubic γ-Fe_2O_3 is not an independent modification in addition to tetragonal γ-Fe_2O_3. Instead, ordered cubic γ-Fe_2O_3 represents an intermediate state upon ordering of vacant octahedral sites from defect spinel γ-Fe_2O_3 with space group $Fd\bar{3}m$ *via* space groups $P4_132/P4_332$ towards tetragonal γ-Fe_2O_3 with space groups $P4_12_12/P4_32_12$. This result was obtained from the crystal symmetry of ordered cubic γ-Fe_2O_3without making further presumptions.

[1] R. M. Cornell, U. Schwertmann, The Iron Oxides, VCH, Weinheim (1996).
[2] E. Tronc, C. Chanéac, J. P. Jolivet, J. Solid State Chem. **93**, 139 (1998).
[3] E. J. W. Verwey, Z. Kristallogr. **91**, 65 (1935).
[4] R. Haul, Th. Schoon, Z. Phys. Chem. **44**, 216 (1939).
[5] P. B. Braun, Nature **170**, 1123 (1952).
[6] G. W. van Oosterhout, C. J. M. Rooijmans, Nature **181**, 44 (1958).
[7] G. A. Ferguson, M. Haas, Phys. Rev. **112**, 1130 (1958).
[8] K. Haneda, A. H. Morrish, Solid State. Commun. **22**, 779 (1977)
[9] B. Gillot, F. Bouton, J. Solid State Chem. **32**, 303 (1980).
[10] K. Egger, W. Feitknecht, Helv. Chim. Acta **45**, 2042 (1962).
[11] D. H. Lindsley, The crystal chemistry and structure of oxide minerals as exemplified by the Fe-Ti-Oxides, in: D. Rumble III (ed.): Oxide minerals. Reviews in Mineralogy 3, p. L4 – L24, Min. Soc. Am., Book Crafters, Inc., Chelsea (1976).
[12] A. N. Shmakov, G. N. Kruyukova, S. V. Tsybulya, A. L. Chuvilin, L. P. Solovyeva, J. Appl. Crystallogr. **28**, 141 (1995).

[13] C. Greaves, J. Solid State Chem. **49**, 325 (1983).
[14] H.-S. Shin, Yoop-hoeji **35**, 1113 (1998).
[15] H.-M. Ho, E. Goo, G. Thomas, J. Appl. Phys. **59**, 1606 (1986).
[16] R. Ueda, K. Hasegawa, J. Phys. Soc. Jpn. **17**, Suppl. B-II, 391 (1961).
[17] K. P. Sinha, A. P. B. Sinha, Z. Anorg. Allg. Chem. **293**, 228 (1958).
[18] D. L. Schulz, G. J. McCarthy, Powder Diffraction **3**, 104 (1988).
[19] P. P. K. Smith, Contrib. Mineral. Petrol. **69**, 249 (1979).
[20] M. Boudeulle, H. Batis-Landoulsi, Ch. Leclercq, P. Vergnon, J. Solid State Chem. **48**, 21 (1983).
[21] U. Schwertmann, R. M. Cornell, Iron Oxides in the Laboratory, VCH, Weinheim u. a. (1991).
[22] A. K. Nikumbh, A. A. Latkar, M. M. Phadke, Thermochim. Acta **219**, 269 (1993).
[23] T. Gonzáles-Carreño, M. P. Morales, M. Garcia, C. J. Serna, Mater. Lett. **18**, 151 (1993).
[24] R. Schrader, G. Büttner Z. Anorg. Allg. Chem. **320**, 205 (1963).
[25] C. Cannas, G. Concas, D. Gatteschi, A. Musinu, G. Piccaluga, C. Sangregiorgio, J. Mater. Chem **12**, 3141 (2002).
[26] J. L. Meijering, in H. Herman (ed.): Advances in Materials Research, p. 1, Wiley, New York (1971).
[27] J. Gegner, G. Hörz, R. Kirchheim, Interface Sci. **5**, 231 (1997).
[28] PDF-2 Data File, JCPDS, Joint Comitee on Powder Diffraction Standards – International Centre for Diffraction Data, Swarthmore, PA (2002).
[29] E. J. Verwey, P. W. Haayman, F. C. Romeijan, J. Chem. Phys. **15**, 181 (1947).
[30] J. P. Morniroli, J. W. Steeds, Ultramic. **45**, 219 (1992).
[31] R. Serneels, M. Snykers, P. Delavignette, R. Grevers, S. Amelinckx, Phys. Stat. Sol. B **58**, 277 (1973).
[32] W. Feitknecht, Mémoires Scientifiques Rev. Métallurg. **42**, 121 (1965).
[33] K. Kelm, W. Mader, Z. Anorg. Allg. Chem. **631**, 2383 (2005).